Article

Optimal Earth Gravity-Assist Maneuvers with an Electric Solar Wind Sail

Lorenzo Niccolai [ID], Marco Bassetto [ID], Alessandro A. Quarta *[ID] and Giovanni Mengali [ID]

Department of Civil and Industrial Engineering, University of Pisa, 56122 Pisa, Italy
* Correspondence: alessandro.antonio.quarta@unipi.it

Abstract: Propellantless propulsive systems such as Electric Solar Wind Sails are capable of accelerating a deep-space probe, only requiring a small amount of propellant for attitude and spin-rate control. However, the generated thrust magnitude is usually small when compared with the local Sun's gravitational attraction. Therefore, the total velocity change necessary for the mission is often obtained at the expense of long flight times. A possible strategy to overcome this issue is offered by an Earth gravity-assist maneuver, in which a spacecraft departs from the Earth's sphere of influence, moves in the interplanetary space, and then re-encounters the Earth with an increased hyperbolic excess velocity with respect to the starting planet. An Electric Solar Wind Sail could effectively drive the spacecraft in the interplanetary space to perform such a particular maneuver, taking advantage of an augmented thrust magnitude in the vicinity of the Sun due to the increased solar wind ion density. This work analyzes Earth gravity-assist maneuvers performed with an Electric Solar Wind Sail based probe within an optimal framework, in which the final hyperbolic excess velocity with respect to the Earth is maximized for a given interplanetary flight time. Numerical simulations highlight the effectiveness of this maneuver in obtaining a final heliocentric orbit with high energy.

Keywords: Electric Solar Wind Sail; Earth gravity-assist maneuvers; trajectory optimization; heliocentric mission design

1. Introduction

An Electric Solar Wind Sail (or E-sail) is a propellantless propulsion system, first proposed by Dr. Pekka Janhunen [1] about twenty years ago, which generates thrust by exploiting the electrostatic interaction between solar wind ions and a charged tether grid [2]. Similarly to other propellantless propulsive systems, such as the more conventional photonic solar sails [3–7] and magnetic sails [8–10], the E-sail is able to operate without requiring any propellant stored onboard to propel the spacecraft in interplanetary space. This feature makes an E-sail a very interesting option for missions requiring a continuous propulsive acceleration, including the generation of displaced non-Keplerian orbits [11,12] and the maintenance of artificial equilibrium points in the Sun–Earth gravitational field [13,14].

Since the magnitude of the propulsive acceleration generated by an E-sail is typically small [15] when compared with that generated by conventional (chemical) thrusters, long flight times are usually necessary to meet the velocity changes required by the scientific mission. Examples of long-lasting missions with E-sail-based thrusts are available in the literature. For example, Quarta et al. [16] discussed the possibility of performing an E-sail-propelled cometary rendezvous and Janhunen et al. [17] analyzed an advanced mission towards Uranus, while other more exotic and fascinating scenarios are represented by in situ studies of the outer regions of the Solar System [18–20]. These mission concepts require the spacecraft to significantly increase its heliocentric velocity in order to reach the target within a reasonable flight time. To that end, a possible option is given by the so-called solar wind assist maneuver [21,22], in which the spacecraft first approaches the Sun with the aim of increasing the E-sail thrust magnitude due to the higher density of solar wind

ions, and then moves towards the outer Solar System regions with a very large inertial velocity magnitude. This strategy is similar to the well-known solar photonic assist [23], when a solar sail approaches the Sun to increase the solar radiation pressure acting on the reflective membrane.

A different method for increasing the spacecraft heliocentric velocity (without using any propellant) is offered by the so-called ΔV-Earth Gravity-Assist (ΔV-EGA) maneuver [24]. To perform such a maneuver, a spacecraft first escapes from the gravitational field of the launch planet and, after a heliocentric phase, re-encounters the starting planet with an increased hyperbolic excess velocity. This allows high-energy final heliocentric orbits to be obtained without requiring an increase in the propellant consumption of the launch vehicle. In its original concept, suitable impulsive maneuvers (provided by chemical thrusters) and intermediate flybys were used for the spacecraft to obtain a desired increase in excess velocity relative to the Earth. The application of ΔV-EGA maneuvers has also been proposed for spacecrafts equipped with low-thrust propulsion systems [25–27], such as electric thrusters [28], solar sails [29,30], or a combination of both [31]. After a ΔV-EGA maneuver and the subsequent re-encounter with Earth, the spacecraft can move towards other planets [32,33] and moons [34], or correct possible orbital injection errors [35]. A further possible application of ΔV-EGA maneuvers consists in obtaining a final heliocentric orbit with a very high orbital energy, which allows the outer Solar System region to be reached in a reasonable time interval. This kind of mission is especially suited for a propellantless propulsive system [36], since a ΔV-EGA maneuver with a Sun approach would be able to combine its effect with the thrust increase induced by the solar wind assist maneuver (or solar photonic assist maneuver in the case of a solar sail spacecraft).

The aim of this work is to analyze the performance a ΔV-EGA maneuver with a spacecraft propelled by an E-sail, in order to quantify its effectiveness in obtaining high-energy heliocentric orbits. The problem is addressed within an optimal framework [37], where the hyperbolic excess velocity relative to the Earth after a given flight time is maximized. The optimal control problem is solved by means of an indirect multiple shooting technique [38], which allows the time histories of the E-sail attitude and the grid voltage to be obtained. To simplify the analysis, the Earth's heliocentric orbit is assumed to be circular, the spacecraft motion is two-dimensional, and the dimensions of Earth's sphere of influence are neglected.

The remainder of the paper is structured as follows. Section 2 describes the mathematical model and formulates the optimal control problem. Section 3 applies the optimal steering law to some potential mission scenarios. Section 4 highlights the main outcomes of the work and suggests possible future developments.

2. Mathematical Model

The analysis of an E-sail-based ΔV-EGA maneuver is made within a two-body heliocentric framework, in which the Earth is assumed to describe a circular orbit around the Sun with radius $r_\oplus \triangleq 1$ au. The spacecraft leaves the Earth's sphere of influence at $t_0 \triangleq 0$ with a hyperbolic excess velocity V_{∞_0} when the E-sail is deployed. The dimensions of the Earth's sphere of influence are neglected here, so that the initial Sun–spacecraft distance is approximately equal to $r_\oplus$. Without loss of generality, the Sun–spacecraft line at the initial time t_0 is chosen as the reference (fixed) direction. The spacecraft motion for $t \geq t_0$ is described with the aid of a heliocentric polar reference frame $\mathcal{T}(O; r, \theta)$, where O is the Sun's center of mass, r is the Sun–spacecraft distance, and θ is a polar angle measured counterclockwise from the reference direction to the Sun–spacecraft line; see Figure 1. The radial and circumferential unit vectors are denoted as $\hat{\boldsymbol{i}}_r$ and $\hat{\boldsymbol{i}}_\theta$, respectively.
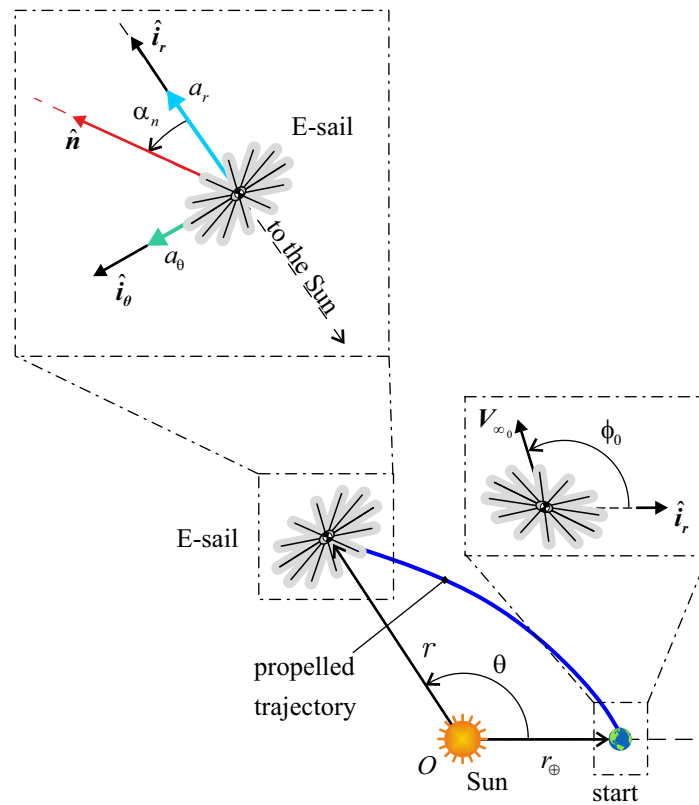
Figure 1. Reference frame and state variables in the proposed mission scenario.

To establish the system dynamics for $t \geq t_0$, a mathematical model that defines the propulsive acceleration vector $\boldsymbol{a}$ generated by the E-sail is necessary. According to Huo et al. [39], the magnitude of $\boldsymbol{a}$ is inversely proportional to r and depends on the E-sail attitude, defined by the orientation of the unit vector $\hat{\boldsymbol{n}}$ normal to the E-sail nominal plane in the direction opposite to the Sun; see Figure 1. In vectorial terms, the E-sail-induced propulsive acceleration is modeled as

$$\boldsymbol{a} = \tau \frac{a_c}{2} \left(\frac{r_\oplus}{r} \right) \left[\hat{\boldsymbol{i}}_r + (\hat{\boldsymbol{i}}_r \cdot \hat{\boldsymbol{n}}) \hat{\boldsymbol{n}} \right] \tag{1}$$

where $\tau \in \{0, 1\}$ is a dimensionless parameter that accounts for the possibility of switching either on ($\tau = 1$) or off ($\tau = 0$) the electron gun that maintains the E-sail electric voltage, and a_c is the spacecraft characteristic acceleration, that is, the classical sail performance parameter defined as the maximum propulsive acceleration at a Sun–spacecraft distance equal to $r_\oplus$. The projection of the propulsive acceleration vector given by Equation (1) along the radial and circumferential directions yields

$$a_r \triangleq \boldsymbol{a} \cdot \hat{\boldsymbol{i}}_r = \tau \frac{a_c}{4} \left(\frac{r_\oplus}{r} \right) [3 + \cos(2\alpha_n)] \tag{2}$$

$$a_\theta \triangleq \boldsymbol{a} \cdot \hat{\boldsymbol{i}}_\theta = \tau \frac{a_c}{4} \left(\frac{r_\oplus}{r} \right) [\sin(2\alpha_n)] \tag{3}$$

where $\alpha_n \in [-\pi/2, \pi/2]$ rad is the E-sail pitch angle, that is, the angle between $\hat{\boldsymbol{n}}$ and $\hat{\boldsymbol{i}}_r$, as sketched in Figure 1. In this work, the switching parameter τ and the pitch angle α_n, which may be varied by the onboard control system [40], are the two control variables of the control problem to be discussed in the next section. Here, we assume that the E-sail can freely vary its attitude with continuity. A more detailed analysis of E-sail attitude dynamics is beyond the scope of this paper, but the interested reader may refer to refs. [41–43].

Using the expressions of $\{a_r, a_\theta\}$ given by Equations (2) and (3), the spacecraft dynamics in $\mathcal{T}$ are written as

$$\dot{r} = u \tag{4}$$

$$\dot{\theta} = v/r \tag{5}$$

$$\dot{u} = -\frac{\mu_\odot}{r^2} + \frac{v^2}{r} + \tau \frac{a_c}{4}\left(\frac{r_\oplus}{r}\right)[3 + \cos(2\alpha_n)] \tag{6}$$

$$\dot{v} = -\frac{u\,v}{r} + \tau \frac{a_c}{4}\left(\frac{r_\oplus}{r}\right)\sin(2\alpha_n) \tag{7}$$

where $\mu_\odot$ is the Sun's gravitational parameter, and u (or v) is the radial (or circumferential) component of the spacecraft heliocentric velocity vector. The dynamical system expressed by Equations (4)–(7) is completed by four initial conditions (subscript 0)

$$r(t_0) \triangleq r_0 = r_\oplus \tag{8}$$

$$\theta(t_0) \triangleq \theta_0 = 0 \tag{9}$$

$$u(t_0) \triangleq u_0 = V_{\infty_0}\cos\phi_0 \tag{10}$$

$$v(t_0) \triangleq v_0 = \sqrt{\frac{\mu_\odot}{r_\oplus}} + V_{\infty_0}\sin\phi_0 \tag{11}$$

where the auxiliary angle $\phi_0 \in (-\pi, \pi]$ rad is measured counterclockwise from the radial unit vector $\hat{i}_r$ to the geocentric velocity vector $\boldsymbol{V}_{\infty_0}$ at t_0; see Figure 1. Note that Equations (10) and (11) may be rewritten, in a compact form, as

$$u_0^2 + \left[v_0 - \sqrt{\frac{\mu_\odot}{r_\oplus}}\right]^2 = V_{\infty_0}^2 \tag{12}$$

Spacecraft Trajectory Optimization

The objective of a ΔV-EGA maneuver is to increase the Earth-relative hyperbolic excess velocity (with respect to its value at the launch phase) when the spacecraft re-encounters the Earth at a given time instant $t = t_f$. The optimal control problem is therefore formulated by maximizing the cost function

$$J \triangleq \sqrt{u_f^2 + \left[v_f - \sqrt{\frac{\mu_\odot}{r_\oplus}}\right]^2} \tag{13}$$

where the subscript f denotes the values at t_f, that is, $u_f \triangleq u(t_f)$ and $v_f \triangleq v(t_f)$. Note that the cost function J represents the hyperbolic excess speed relative to the Earth at the end of the ΔV-EGA maneuver, that is, when the spacecraft re-enters the Earth's sphere of influence. The constraints on the spacecraft state variables at time t_f are therefore

$$r(t_f) \triangleq r_f = r_\oplus \tag{14}$$

$$\theta(t_f) \triangleq \theta_f = \theta_0 + \sqrt{\frac{\mu_\odot}{r_\oplus^3}}\,t_f \equiv \sqrt{\frac{\mu_\odot}{r_\oplus^3}}\,t_f \tag{15}$$

The optimal control problem aimed at maximizing the value of J in Equation (13) is solved by means of an indirect method [37]. To this end, first introduce a set of costate variables $\{\lambda_r, \lambda_\theta, \lambda_u, \lambda_v\}$ associated with the physical state variables $\{r, \theta, u, v\}$, the dynamics of which are given by Equations (4)–(7). Then, define the control Hamiltonian function $\mathcal{H}$ as [44]

$$\mathcal{H} = \lambda_r\, u + \frac{\lambda_\theta\, v}{r} + \lambda_u \left(\frac{v^2}{r} - \frac{\mu_\odot}{r^2} \right) - \frac{\lambda_v\, u\, v}{r} + \lambda_u\, a_r + \lambda_v\, a_\theta \tag{16}$$

where $\{a_r, a_\theta\}$ are given by Equations (2) and (3). The time variation of the costates is described by the Euler–Lagrange equations, viz.

$$\dot{\lambda}_r = -\frac{\partial H}{\partial r} = \frac{v\, \lambda_\theta}{r^2} - \lambda_u \left(\frac{2\, \mu_\odot}{r^3} - \frac{v^2}{r^2} - \frac{a_r}{r} \right) - \lambda_v \left(\frac{u\, v}{r^2} - \frac{a_\theta}{r} \right) \tag{17}$$

$$\dot{\lambda}_\theta = -\frac{\partial H}{\partial \theta} = 0 \tag{18}$$

$$\dot{\lambda}_u = -\frac{\partial H}{\partial u} = \frac{v\, \lambda_v}{r} - \lambda_r \tag{19}$$

$$\dot{\lambda}_v = -\frac{\partial H}{\partial v} = \frac{u\, \lambda_v - 2\, v\, \lambda_u - \lambda_\theta}{r} \tag{20}$$

In particular, Equation (18) states that λ_θ is a constant of motion.

The trajectory that maximizes J may be found by enforcing the optimal steering law $\{\alpha_n = \alpha_n^\star(t), \tau = \tau^\star(t)\}$, which defines the optimal time variations of the two control parameters. According to Pontryagin's maximum principle, the optimal steering law maximizes, at any time, the Hamiltonian function given by Equation (16). Starting from the results of ref. [39], the optimal steering law may be written as

$$\alpha_n \equiv \alpha_n^\star = \frac{\alpha_p}{2} \tag{21}$$

$$\tau \equiv \tau^\star = \frac{1 + \text{sign}\left(1 + 3\cos\alpha_p\right)}{2} \tag{22}$$

where $\text{sign}(\square)$ denotes the signum function, and the auxiliary angle $\alpha_p \in [-\pi/2, \pi/2]$ rad is defined as

$$\alpha_p \triangleq \arctan\left(\frac{\lambda_v}{\lambda_u} \right) \tag{23}$$

Having defined the optimal steering law through Equations (21) and (22), the spacecraft trajectory that maximizes the cost function J is obtained by solving the associated two-point boundary value problem (TPBVP). To this end, the dynamical Equations (4)–(7) and the Euler–Lagrange Equations (17)–(20) are numerically integrated in double precision using a variable-order Adams–Bashforth–Moulton solver scheme [45,46], with initial conditions given by Equations (8), (9) and (12), and terminal conditions expressed by Equations (14) and (15).

The set of boundary conditions is completed by the transversality condition [44], to be enforced both at $t = t_0$ and $t = t_f$, that is

$$\lambda_{u_0} = \lambda_{v_0}\, \cot\phi_0 \tag{24}$$

$$\lambda_{u_f} = \frac{u_f}{J} \tag{25}$$

$$\lambda_{v_f} = \frac{v_f - \sqrt{\mu_\odot / r_\oplus}}{J} \qquad (26)$$

where $\lambda_{u_0} \triangleq \lambda_u(t_0)$, $\lambda_{v_0} \triangleq \lambda_v(t_0)$, $\lambda_{u_f} \triangleq \lambda_u(t_f)$, and $\lambda_{v_f} \triangleq \lambda_v(t_f)$, while J is given by Equation (13). Note that, according to Equation (24), the initial values of λ_u and λ_v are not independent but are related through the auxiliary angle ϕ_0.

Equations (24)–(26) complete the set of eight boundary conditions necessary to fully define the TPBVP. A multiple shooting procedure is applied to obtain the values of the set $\{\phi_0, \lambda_{r_0}, \lambda_{\theta_0}, \lambda_{v_0}\}$. Note that Equation (24) assumes that $\phi_0 \notin \{0, \pi\}$ rad, that is, the spacecraft velocity relative to the Earth at t_0 is not aligned with the Sun–spacecraft line; see Figure 1. In the special case when $\phi_0 \in \{0, \pi\}$ rad, the condition that relates λ_{u_0} and λ_{v_0} is no longer valid, and the multiple shooting procedure gives the set of initial values of the costates $\{\lambda_{r_0}, \lambda_{\theta_0}, \lambda_{u_0}, \lambda_{v_0}\}$ as outputs.

3. Case Study

The previously described methodology to find the optimal ΔV-EGA trajectory is now simulated in some potential mission applications. In the following analysis, in analogy with previous works [29–31,36], it is assumed that the spacecraft leaves the Earth's sphere of influence with hyperbolic excess velocity in the set $V_{\infty_0} = \{0.5, 1, 1.5, 2, 2.5, 3\}$ km/s. At t_0, the spacecraft deploys an E-sail with a characteristic acceleration in the set $a_c \in \{0.1, 0.2, 0.5, 1\}$ mm/s^2. These values of a_c are compatible with a near- and mid-term technology level [15,47].

A ΔV-EGA maneuver is then started, with the aim of maximizing the hyperbolic excess speed relative to the Earth at its re-encounter, after a flight time $t_f = 1$ year. The performance parameter P, defined as

$$P \triangleq \frac{J - V_{\infty_0}}{V_{\infty_0}}, \qquad (27)$$

is used to quantify the relative increase in hyperbolic excess velocity obtained from the ΔV-EGA maneuver. In particular, note that $P = 0$ corresponds to when the ΔV-EGA maneuver gives no increase in the hyperbolic excess velocity, while $P = 1$ indicates that the final excess velocity is twice its initial value.

Figure 2 shows the values of P obtained after a flight time of 1 year as functions of the initial hyperbolic excess velocity V_{∞_0} and the E-sail characteristic acceleration a_c. It is evident that, regardless of the E-sail performance level, the ΔV-EGA maneuver is more effective in increasing the hyperbolic excess velocity when its initial value is small. In those cases, indeed, the final values are several times larger than the initial values. However, the ΔV-EGA contribution is remarkable (on the order of some kilometers per second), even for large values of V_{∞_0}.

Figures 3–6 show some examples of the optimal ΔV-EGA maneuvers with $t_f = 1$ year, $V_{\infty_0} = 1$ km/s, and different a_c and show the spacecraft trajectory and the corresponding optimal steering law of the pitch angle. The steering law of the switching parameter is not shown because $\tau^\star \equiv 1$ for the whole flight in all of the considered scenarios. This is not surprising, because the aim of the ΔV-EGA maneuver is to obtain a large value of J, which requires the E-sail to be always switched on during the approach phase towards the Sun.
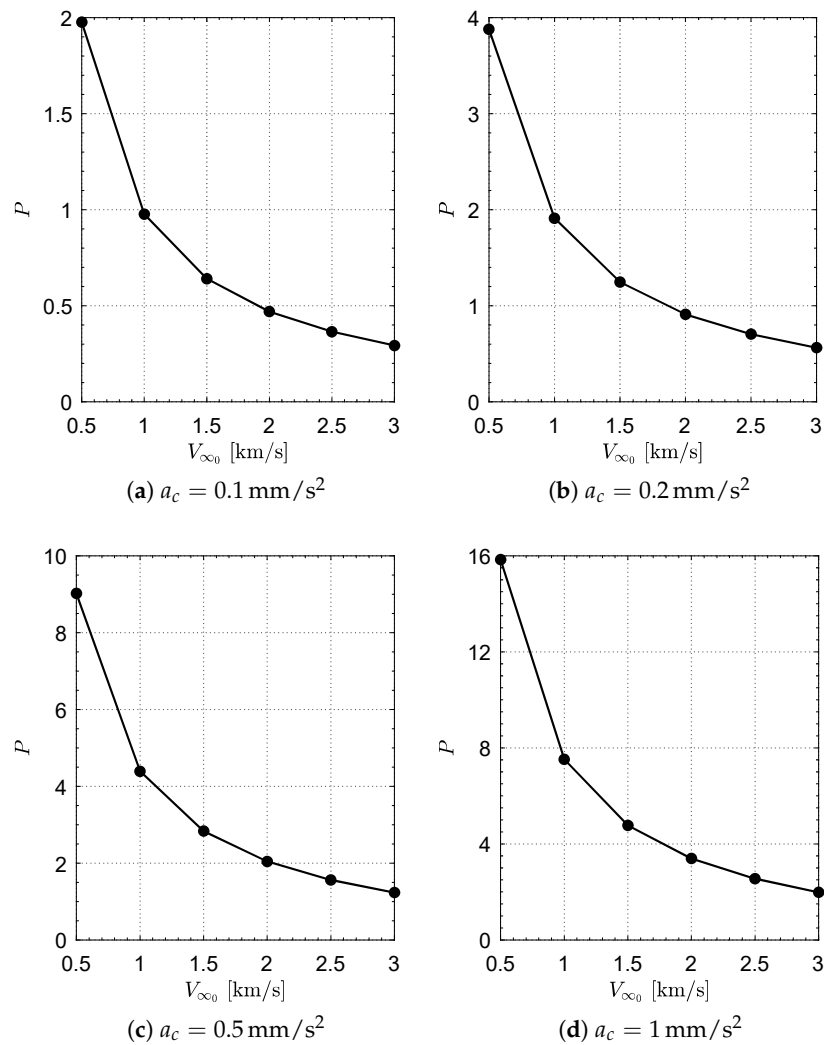
Figure 2. ΔV-EGA performance parameters P as functions of V_{∞_0} and a_c for a flight time of 1 year.
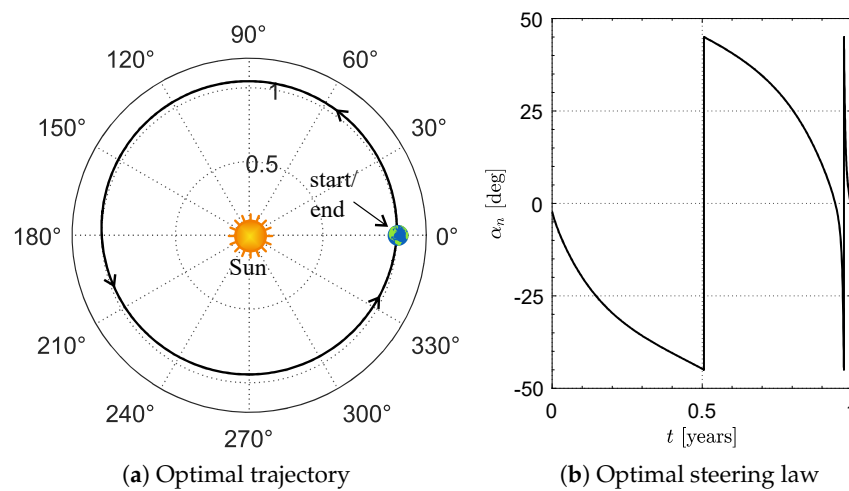
Figure 3. ΔV-EGA maneuver trajectory and corresponding optimal steering law $\alpha_n = \alpha_n^\star(t)$ for $a_c = 0.1\,\mathrm{mm/s^2}$, $V_{\infty_0} = 1\,\mathrm{km/s}$, and $t_f = 1\,\mathrm{year}$.

(**a**) Optimal trajectory　　　　　　　(**b**) Optimal steering law
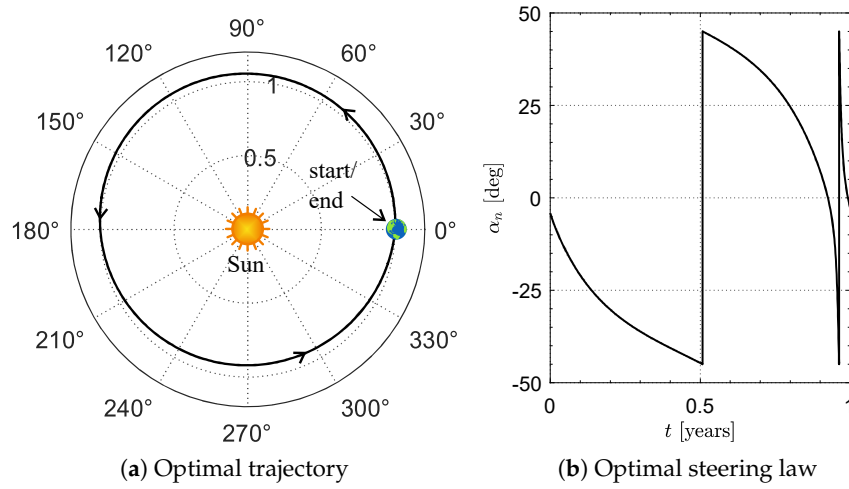
Figure 4. ΔV-EGA maneuver trajectory and corresponding optimal steering law $\alpha_n = \alpha_n^\star(t)$ for $a_c = 0.2\,\mathrm{mm/s^2}$, $V_{\infty_0} = 1\,\mathrm{km/s}$, and $t_f = 1\,\mathrm{year}$.

(**a**) Optimal trajectory　　　　　　　(**b**) Optimal steering law
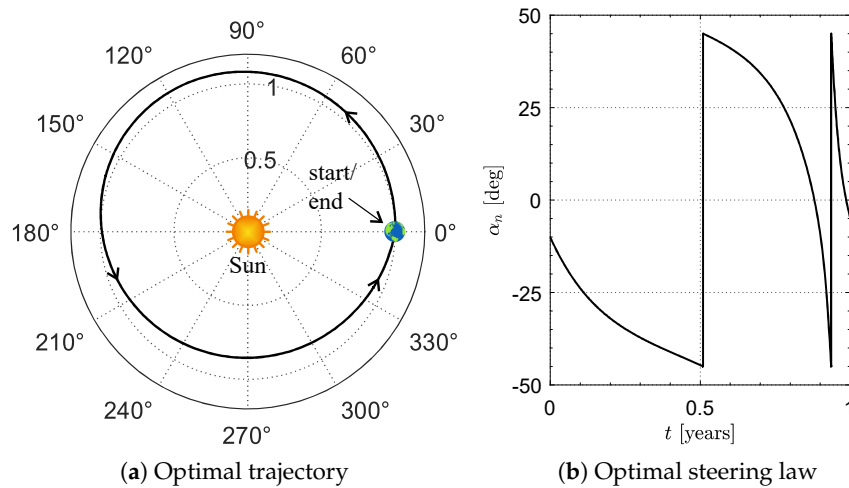
Figure 5. ΔV-EGA maneuver trajectory and corresponding optimal steering law $\alpha_n = \alpha_n^\star(t)$ for $a_c = 0.5\,\mathrm{mm/s^2}$, $V_{\infty_0} = 1\,\mathrm{km/s}$, and $t_f = 1\,\mathrm{year}$.

(**a**) Optimal trajectory　　　　　　　(**b**) Optimal steering law
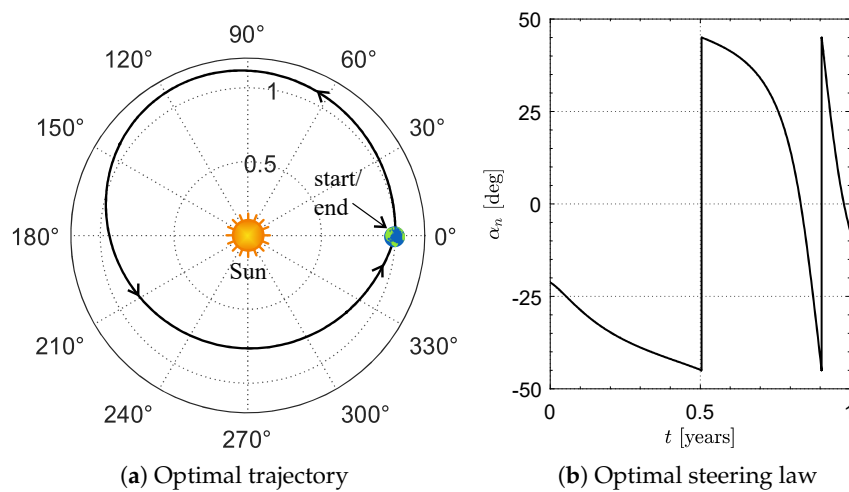
Figure 6. ΔV-EGA maneuver trajectory and corresponding optimal steering law $\alpha_n = \alpha_n^\star(t)$ for $a_c = 1\,\mathrm{mm/s^2}$, $V_{\infty_0} = 1\,\mathrm{km/s}$, and $t_f = 1\,\mathrm{year}$.

4. Conclusions

This paper analyzed the performance of an Earth gravity-assist maneuver for a spacecraft propelled by an Electric Solar Wind Sail. To this end, an optimal control problem was formulated with the aim of finding the steering law that maximizes the spacecraft hyperbolic excess velocity when it re-encounters the Earth. The results, obtained with an indirect multiple shooting technique, highlight that an Earth gravity-assist maneuver is able to provide a significant increment in the hyperbolic excess velocity relative to the Earth, and the relative increase is larger when the initial excess velocity is smaller. Accordingly, this strategy could allow high-energy heliocentric orbits to be obtained, even when the initial excess velocity provided by the launcher is small, thus opening the possibility of reaching large heliocentric distances in reasonable flight times. Future work will concentrate on a refinement of the model discussed here by accounting for the Earth's gravity and the eccentricity and mutual inclination of the planetary heliocentric orbits.

Author Contributions: Conceptualization, L.N. and M.B.; methodology, L.N.; software, L.N. and A.A.Q.; writing—original draft preparation, L.N., A.A.Q. and G.M.; writing—review and editing, G.M. and A.A.Q. All authors have read and agreed to the published version of the manuscript.

Institutional Review Board Statement: Not applicable.

Informed Consent Statement: Not applicable.

Data Availability Statement: Not applicable.

Conflicts of Interest: The authors declare no conflict of interest.

Notation

$\boldsymbol{a}$	propulsive acceleration vector [mm/s^2]
a_c	characteristic acceleration [mm/s^2]
a_r	radial component of $\boldsymbol{a}$ [mm/s^2]
a_θ	circumferential component of $\boldsymbol{a}$ [mm/s^2]
$\mathcal{H}$	Hamiltonian function
J	cost function; see Equation (13) [km/s]
$\hat{\boldsymbol{\imath}}_r$	radial unit vector
$\hat{\boldsymbol{\imath}}_\theta$	circumferential unit vector
P	dimensionless performance parameter, see Equation (27)
r	Sun–spacecraft distance [au]
$r_\oplus$	Sun–Earth distance [au]
t	time [days]
$\mathcal{T}$	polar reference frame
u	radial component of the spacecraft velocity [km/s]
$\boldsymbol{V}_\infty$	spacecraft velocity vector relative to the Earth [km/s] (with $V_\infty = \|\boldsymbol{V}_\infty\|$)
v	circumferential component of the spacecraft velocity [km/s]
α_n	E-sail pitch angle [rad]
α_p	auxiliary angle; see Equation (23) [rad]
θ	polar angle [rad]
λ_r	dimensionless costate variable adjoint to r
λ_u	dimensionless costate variable adjoint to u
λ_v	dimensionless costate variable adjoint to v
λ_θ	dimensionless costate variable adjoint to θ
$\mu_\odot$	Sun's gravitational parameter [km^3/s^2]
τ	dimensionless switching parameter
Subscripts	
0	initial value
f	final value
Superscripts	
$\star$	optimal value

References

1. Janhunen, P. Electric sail for spacecraft propulsion. *J. Propuls. Power* **2004**, *20*, 763–764. [CrossRef]
2. Bassetto, M.; Niccolai, L.; Quarta, A.A.; Mengali, G. A comprehensive review of Electric Solar Wind Sail concept and its applications. *Prog. Aerosp. Sci.* **2022**, *128*, 1–27. [CrossRef]
3. Fu, B.; Sperber, E.; Eke, F. Solar sail technology—A state of the art review. *Prog. Aerosp. Sci.* **2016**, *86*, 1–19. [CrossRef]
4. Gong, S.; Macdonald, M. Review on solar sail technology. *Astrodynamics* **2019**, *3*, 93–125. [CrossRef]
5. Zhang, F.; Gong, S.; Baoyin, H. Three-axes attitude control of solar sail based on shape variation of booms. *Aerospace* **2021**, *8*, 198. [CrossRef]
6. Zou, J.; Li, D.; Wang, J.; Yu, Y. Experimental study of measuring the wrinkle of solar sails. *Aerospace* **2022**, *9*, 289. [CrossRef]
7. Bassetto, M.; Niccolai, L.; Quarta, A.A.; Mengali, G. Logarithmic spiral trajectories generated by solar sails. *Celest. Mech. Dyn. Astron.* **2018**, *130*, 18.1–18.24. [CrossRef]
8. Andrews, D.G.; Zubrin, R.M. Magnetic sails and interstellar travel. *J. Br. Interplanet. Soc.* **1990**, *43*, 265–272.
9. Zubrin, R.M. The use of magnetic sails to escape from low Earth orbit. *J. Br. Interplanet. Soc.* **1992**, *46*, 3–10. [CrossRef]
10. Bassetto, M.; Quarta, A.A.; Mengali, G. Magnetic sail-based displaced non-Keplerian orbits. *Aerosp. Sci. Technol.* **2019**, *92*, 363–372. [CrossRef]
11. Niccolai, L.; Quarta, A.A.; Mengali, G. Electric sail elliptic displaced orbits with advanced thrust model. *Acta Astronaut.* **2017**, *138*, 503–511. [CrossRef]
12. Niccolai, L.; Anderlini, A.; Mengali, G.; Quarta, A.A. Electric sail displaced orbit control with solar wind uncertainties. *Acta Astronaut.* **2019**, *162*, 563–573. [CrossRef]
13. Aliasi, G.; Mengali, G.; Quarta, A.A. Artificial Equilibrium Points for an Electric Sail with Constant Attitude. *J. Spacecr. Rocket.* **2013**, *50*, 1295–1298. [CrossRef]
14. Niccolai, L.; Caruso, A.; Quarta, A.A.; Mengali, G. Artificial collinear Lagrangian point maintenance with electric solar wind sail. *IEEE Trans. Aerosp. Electron. Syst.* **2020**, *56*, 4467–4477. [CrossRef]
15. Janhunen, P.; Quarta, A.A.; Mengali, G. Electric solar wind sail mass budget model. *Geosci. Instrum. Methods Data Syst.* **2013**, *2*, 85–95. [CrossRef]
16. Quarta, A.A.; Mengali, G.; Janhunen, P. Electric sail option for cometary rendezvous. *Acta Astronaut.* **2016**, *127*, 684–692. [CrossRef]
17. Janhunen, P.; Lebreton, J.P.; Merikallio, S.; Paton, M.; Mengali, G.; Quarta, A.A. Fast E-sail Uranus entry probe mission. *Planet. Space Sci.* **2014**, *104*, 141–146. [CrossRef]
18. Sanchez-Torres, A. Propulsive force in electric solar sails for missions in the heliosphere. *IEEE Trans. Plasma Sci.* **2019**, *47*, 1657–1662. [CrossRef]
19. Mengali, G.; Quarta, A.A. Trajectory analysis and optimization of Hesperides mission. *Universe* **2022**, *8*, 364. [CrossRef]
20. Mengali, G.; Quarta, A.A.; Janhunen, P. Considerations of electric sailcraft trajectory design. *J. Br. Interplanet. Soc.* **2008**, *61*, 326–329.
21. Huo, M.Y.; Mengali, G.; Quarta, A.A. Mission design for an interstellar probe with E-sail propulsion system. *JBIS—J. Br. Interplanet. Soc.* **2015**, *68*, 128–134.
22. Quarta, A.A.; Mengali, G. Electric sail mission analysis for outer solar system exploration. *J. Guid. Control Dyn.* **2010**, *33*, 740–755. [CrossRef]
23. Leipold, M.; Wagner, O. 'Solar photonic assist' trajectory design for solar sail missions to the outer solar system and beyond. In Proceedings of the AAS/GSFC International Symposium on Flight Dynamics, Greenbelt, MD, USA, 11–15 May 1998.
24. Hollenbeck, G.R. New flight techniques for outer planet missions. In Proceedings of the AAS/AIAA Astrodynamics Specialist Conference, Nassau, Bahamas, 28–30 July 1975.
25. Atkins, K.L.; Sauer, C.G., Jr.; Flandro, G.A. Solar electric propulsion combined with Earth gravity assist: A new potential for planetary exploration. In Proceedings of the AIAA/AAS Astrodynamics Conference, San Diego, CA, USA, 13–16 September 1976. [CrossRef]
26. Kawaguchi, J. Solar electric propulsion leverage: Electric delta-VEGA (EDVEGA) scheme and its application. In Proceedings of the AAS/AIAA Space Flight Mechanics Meeting, Santa Barbara, CA, USA, 11–15 February 2001.
27. Kawaguchi, J. Performance evaluation for the electric Delta-V Earth Gravity Assist (EDVEGA) scheme. In Proceedings of the AIAA/AAS Astrodynamics Specialist Conference and Exhibit, Monterey, CA, USA, 5–8 August 2002. [CrossRef]
28. O'Reilly, D.; Herdrich, G.; Kavanagh, D.F. Electric propulsion methods for small satellites: A review. *Aerospace* **2021**, *8*, 22. [CrossRef]
29. Quarta, A.A.; Bianchi, C.; Niccolai, L.; Mengali, G. Optimal V_∞ leveraging maneuvers using gray solar sail. *Aerosp. Sci. Technol.* **2022**, *126*, 1–9. [CrossRef]
30. Quarta, A.A.; Bianchi, C.; Niccolai, L.; Mengali, G. Solar sail-based V-infinity leveraging missions from elliptic orbit. *Aerosp. Sci. Technol.* **2022**, *130*, 1–9. [CrossRef]
31. Takao, Y.; Chujo, T. Delta-V Earth-gravity assist trajectories with hybrid solar electric-photonic propulsion. *J. Guid. Control Dyn.* **2022**, *45*, 162–170. [CrossRef]
32. Sims, J.A.; Longuski, J.M. Analysis of V_∞ leveraging for interplanetary missions. In Proceedings of the AIAA/AAS Astrodynamics Conference, Scottsdale, AZ, USA, 1–3 August 1994. [CrossRef]

33. Sims, J.A.; Longuski, J.M.; Staugler, A.J. V_∞ leveraging for interplanetary missions: Multiple-revolution orbit techniques. *J. Guid. Control Dyn.* **1997**, *20*, 409–415. [CrossRef]

34. Brinckerhoff, A.T.; Russell, R.P. Pathfinding and V-Infinity leveraging for planetary moon tour missions. In Proceedings of the 19th AAS/AIAA Space Flight Mechanics Meeting, Savannah, GA, USA, 8–12 February 2009; Volume 134.

35. Ozaki, N.; Chikazawa, T.; Kakihara, K.; Ishikawa, A.; Kawakatsu, Y. Extended robust planetary orbit insertion method under probabilistic uncertainties. *J. Spacecr. Rocket.* **2020**, *57*, 1153–1164. [CrossRef]

36. Bianchi, C.; Niccolai, L.; Mengali, G. Solar sail-based deep space transfers using V-infinity leveraging maneuvers. In Proceedings of the 73rd International Astronautical Congress (IAC), Paris, France, 18–22 September 2022.

37. Morante, D.; Sanjurjo Rivo, M.; Soler, M. A survey on low-thrust trajectory optimization approaches. *Aerospace* **2021**, *8*, 88. [CrossRef]

38. Shi, J.; Wang, J.; Su, L.; Ma, Z.; Chen, H. A neural network warm-started indirect trajectory optimization method. *Aerospace* **2022**, *9*, 435. [CrossRef]

39. Huo, M.Y.; Mengali, G.; Quarta, A.A. Electric sail thrust model from a geometrical perspective. *J. Guid. Control Dyn.* **2018**, *41*, 735–741. [CrossRef]

40. Janhunen, P.; Toivanen, P.K.; Polkko, J.; Merikallio, S.; Salminen, P.; Haeggström, E.; Seppänen, H.; Kurppa, R.; Ukkonen, J.; Kiprich, S.; et al. Electric solar wind sail: Toward test missions. *Rev. Sci. Instrum.* **2010**, *81*, 111301. [CrossRef] [PubMed]

41. Toivanen, P.K.; Janhunen, P. Thrust vectoring of an electric solar wind sail with a realistic sail shape. *Acta Astronaut.* **2017**, *131*, 145–151. [CrossRef]

42. Liu, F.; Hu, Q.; Liu, Y. Attitude dynamics of electric sail from multibody perspective. *J. Guid. Control Dyn.* **2018**, *41*, 2633–2646. [CrossRef]

43. Bassetto, M.; Mengali, G.; Quarta, A.A. Attitude dynamics of an electric sail model with a realistic shape. *Acta Astronaut.* **2019**, *159*, 250–257. [CrossRef]

44. Bryson, A.E.; Ho, Y.C. *Applied Optimal Control: Optimization, Estimation and Control*; Hemisphere Publishing Corporation: New York, NY, USA, 1975; Chapter 2, pp. 87–89.

45. Shampine, L.F.; Gordon, M.K. *Computer Solution of Ordinary Differential Equations: The Initial Value Problem*; W. H. Freeman & Co., Ltd.: San Francisco, CA, USA, 1975; Chapter 10. ISBN 0-716-70461-7.

46. Shampine, L.F.; Reichelt, M.W. The MATLAB ODE Suite. *SIAM J. Sci. Comput.* **1997**, *18*, 1–22. [CrossRef]

47. Slavinskis, A.; Janhunen, P.; Toivanen, P.; Muinonen, K.; Penttilä, A.; Granvik, M.; Kohout, T.; Gritsevich, M.; Pajusalu, M.; Sunter, I.; et al. Nanospacecraft fleet for multi-asteroid touring with electric solar wind sails. In Proceedings of the IEEE Aerospace Conference Proceedings, Big Sky, MT, USA, 3–10 March 2018; Volume 2018; pp. 1–20. [CrossRef]